Mitigating Domain Mismatch in Face Recognition Using Style Matching

Chun-Hsien Lin, Bing-Fei Wu

Abstract

Despite outstanding performance on public benchmarks, face recognition still suffers due to domain mismatch between training (source) and testing (target) data. Furthermore, these domains are not shared classes, which complicates domain adaptation. Since this is also a fine-grained classification problem which does not strictly follow the low-density separation principle, conventional domain adaptation approaches do not resolve these problems. In this paper, we formulate domain mismatch in face recognition as a style mismatch problem for which we propose two methods. First, we design a domain discriminator with human-level judgment to mine target-like images in the training data to mitigate the domain gap. Second, we extract style representations in low-level feature maps of the backbone model, and match the style distributions of the two domains to find a common style representation. Evaluations on verification and open-set and closed-set identification protocols show that both methods yield good improvements, and that performance is more robust if they are combined. Our approach is competitive with related work, and its effectiveness is verified in a practical application.

Keywords: face recognition, domain adaptation, style transfer, Sinkhorn algorithm, optimal transport

1. Introduction

Face recognition is an efficient tool for identity authentication. When implemented using deep learning, its performance is nearly perfect on public benchmarks, and it can be used in applications as varied as social media, surveillance, police, and military. However, as shown persuasively in Phillips [1], in real-world deployments, powerful face recognition models usually exhibit poor performance, regardless of the amount of training data.

This is primarily due to domain mismatch, that is, the mismatch between the training data (the source domain) and testing data (target domain) distributions. Such mismatch can be caused by differences in illumination, race, gender, or age. One solution is to fine-tune the model on the target domain with supervised training, but labeling is expensive, and it is impossible to collect labeled data that covers all possible scenarios. The problem is thus how best to adapt the model by leveraging unlabeled data in the target domain.

Although many studies have been conducted on this problem, most assume that the domains are shared classes. The premise of face recognition, however, is the opposite. In general, identities in a scenario do not constitute a training dataset, which leads to an unique problem in face recognition. Therefore, of the few studies on domain mismatch for face recognition [2, 3, 4, 5, 6, 7, 8], most adopt domain adaptation approaches. According to Yosinski et al. [9], for convolutional neural networks (CNNs), as lower layers are more transferable, the main idea for classical domain adaptation is to fine-tune parameters by aligning the feature distributions of the two domains in higher layers. They achieve modest improvements under the low-density separation assumption. In contrast to objects, the contour variation among human faces is low, which means that face recognition is a kind of fine-grained classification problem. Since feature distributions of unseen identities do not necessarily satisfy the low-density separation assumption, domain mismatch in face recognition should be accounted for at the texture level.

One technique for domain adaptation is to adapt source images to appear as if drawn from the target domain [10, 11, 12] and to fine-tune the model with the transferred images to reduce the domain gap. With the advance of generative adversarial networks (GAN) [13], it is possible to synthesize precise facial images [14, 15, 16]. Thus it would seem that GANs could be used to reduce face recognition domain mismatch, but using GANs to transfer source images could lead to two problems. First, if non-face images are generated, learning would be harmed. Second, the styles in both domains should be diverse, but as style is not easily defined, it is difficult to determine which target style a source image should be transferred to. Transferring each source image to the styles of all target images would incur a complexity of $O(N^2)$. The GAN must be large enough to generate high-quality images, and there must be a sufficient number of identities and images in the training data. This would however preclude the transfer of all the source images in a reasonable amount of time.

In this paper, we propose a feasible method for style-based (or, equiva-

2

lently, texture-level) model adaptation. We follow Zhang et al. [17] in adopting a domain discriminator with human-level judgment to evaluate the similarity of a source image to the target domain. Also, per Chu et al. [18], Wu et al. [19], and Liu et al. [20], we utilize evaluations to up-weight source images that are visually similar to target images. This adaptation mechanism is called perceptual scoring (PS). The style of an image can be represented by feature map statistics from lower to higher CNN layers [21, 22, 23, 15]. We adopt Sinkhorn divergence [24, 25, 26, 27, 28, 29, 30] to align the style distributions of the source and target domains as if the convolutional layers are learned to produce a common style space in which source and target images are visually similar. This results in shallow-layer feature maps which are domain-invariant. We term this approach *style matching* (SM).

To evaluate the performance of the proposed approaches, we conduct evaluations on IJB-A/B/C [31, 32, 33] since they provide comprehensive face verification, closed-set identification, and open-set identification protocols, facilitating evaluations under various scenarios. The effectiveness of our approach is competitive with that of related work on domain adaptation for face recognition. Moreover, to understand whether the proposed approaches are capable of solving real world problems, we apply them to a surveillance application in the library of National Chiao Tung University (NCTU). The testing results show that the proposed approaches can improves a baseline model by a large margin.

The contributions in this research can be summarized as follows:

- We conduct a comprehensive study of domain adaptation for face recognition, showing that most domain adaptation techniques do not apply to face recognition. If adaptation algorithms for face recognition are designed at the texture level, domain mismatch can be formulated as a style mismatch problem.

- We propose perceptual scoring with human-level judgment to enhance the learning of visually target-like source images. Style matching adapts the model by learning a common style space in which the style distributions of both domains are confused.

- We conduct comprehensive testing protocols to cover all possible applications of face recognition to evaluate models objectively. Experiment results demonstrate the competitiveness of the proposed approaches.

- We apply the proposed approaches to a real scenario, and show the significant improvements compared with the baseline.

The rest of this paper is structured as follows: In Section 2, we briefly review related work on face recognition and domain adaptation. Then, in Section 3, we describe in detail the proposed approaches, and in Section 4 we explain the evaluation protocols for different scenarios. In Section 5, we explain the experimental settings, analyze the testing results, and compare these with prior work. We conclude in Section 6.

2. Related Work

2.1. Face Recognition

After deep CNN-based face recognition [34] successfully surpassed conventional methods by a large margin on a famous benchmark [35], this became the major backbone of face recognition [36]. DeepID [37, 38, 39] improves classification loss with contrastive loss [40] to learn a discriminative embedding space. Triplet loss [41] separates positive pairs from negative samples via a distance measure, and is free from classification loss. Learning embeddings without a classifier is known as metric learning [42]. Such a learning strategy relies heavily on good data mining methods. Schroff et al. [41] adopt hard sample mining to learn informative triplets. Center loss [43] reduces intra-class variation by regressing features to their cluster centers. To further separate inter-class samples, many margin penalty losses have been proposed, including SphereFace [44], CosFace [45], and ArcFace [46]. As presented in Deng et al. [46], classification loss with a suitable margin penalty significantly improves performance. Thus determining a good margin is an active research focus. Liu et al. [47] learn margins by maximizing them in total loss. Fair loss [48] involves using a policy network trained by reinforcement learning to control margins according to the samples in the current batch. Huang et al. [49] change the loss adaptively by evaluating the relation between intra- and inter-class similarities.

Despite the nearly perfect accuracy achieved by these methods, their performance depends on huge labeled datasets to achieve better generalization, and thus methods in this line of research cannot be used to account for domain mismatch.

2.2. Domain Adaptation

The aim of domain adaptation is to leverage unlabeled data to fine-tune a trained model for the target domain; source data labels are assumed to be available [50]. The main challenge with domain adaptation is domain mismatch, that is, dissimilar distributions for the two domains, which degrades model performance in the target domain. To eliminate this domain gap, some focus on modifying the classifier's decision boundary [18], while others focus on learning an embedding space in which the distributions of the two domains are aligned [51, 52, 53, 19, 54, 55, 56]. Target-domain performance can be refined by observing the low-density separation principle. Since aligning distributions does not fully satisfy the assumption that domains are shared classes, studies have been conducted on developing better distribution matching methods. Maximum mean discrepancy (MMD) has been widely adopted for domain adaptation [51, 53]. By mapping features to a reproducing kernel Hilbert space (RKHS), we can estimate the domain discrepancy through the squared distance between kernel mean embeddings. In Long et al. [51, 53], MMD is used to match feature distributions on deeper CNN layers. Yan et al. [57] weight MMD by class information to better match the feature distributions. Although MMD is simple and effective, it tends to focus on matching high-density regions [27]. The success of GANs [13] has revealed adversarial learning as another option [54, 55, 56]: a domain discriminator is created to judge the domain of each sample. For training, this results in learning an embedding space to fool the domain discriminator, which results in the distributions being confused. Although adversarial learning based approaches achieve improved performance, they still involve the training of extra parameters (for the discriminator). Also, in many approaches, the two models are trained interactively, which complicates the setting of proper hyperparameters for training.

2.3. Domain Adaptation for Face Recognition

Face recognition is a fine-grained classification problem for which the classes (identities) in the source and target domains are not the same. Hence, conventional domain adaptation methods cannot be used for face recognition. There is a paucity of research on domain adaptation for face recognition.

2.3.1. Distribution Matching

Distributions can be matched by MMD [2] or adversarial learning [6, 7] to produce a distribution-confused embedding space. However, these ap-

proaches are not sufficient for face recognition since inter-class embeddings may not be separable in target domain.

2.3.2. Clustering

To make up for the shortcomings of distribution matching, clustering is used to assign pseudo labels in the target domain. In Wang and Deng [3], a target-domain classifier is trained using pseudo labels. Following the low-density separation principle, Wang et al. [4] use mutual information loss to categorize target-domain embeddings. Leveraging frame consistency in video face recognition, Arachchilage and Izquierdo [5] better estimate positive and negative pairs of target images. After clustering and mining, the model is fine-tuned using a modified version of triplet loss. Similar work is described in Arachchilage and Izquierdo [8]. As clustering-based methods rely on the target domain priors, hyperparameters must be determined before clustering, which is difficult in practice.

2.3.3. Instance Normalization

In work on style transfer [21, 22, 23, 15], instance normalization is used for style normalization. This could also be a way to learn a domain-invariant model. Li et al. [58] remove bias by taking the mean and standard deviation from the target domain as batch normalization parameters. Qing et al. [59] combine instance and batch normalization (IBN) to improve cross-domain recognition. Nam et al. [60] propose batch-instance normalization (BIN), summing instance and batch normalization with an optimal ratio; they thus yield superior results by learning the ratio between two operators. In Qian et al. [61], the IBN layer is adopted as the domain adaptation layer, and the ratio between batch and instance normalization is determined by the domain statistics. Drawing from these studies, Jin et al. [62] propose style normalization and restitution (SNR), extracting domain-invariant features and preserving task-relevant information to further improve performance. However, these approaches necessitate changes to the network architecture that incur a far greater computational complexity.

3. Proposed Approach

With domain adaptation, the training dataset is taken as the source domain, denoted by $X^s = \{x_i^s, y_i^s\}_{i=1}^{n^s}$, and the testing dataset is taken as the target domain, denoted by $X^t = \{x_j^t\}_{j=1}^{n^t}$. There are n^s images in the source
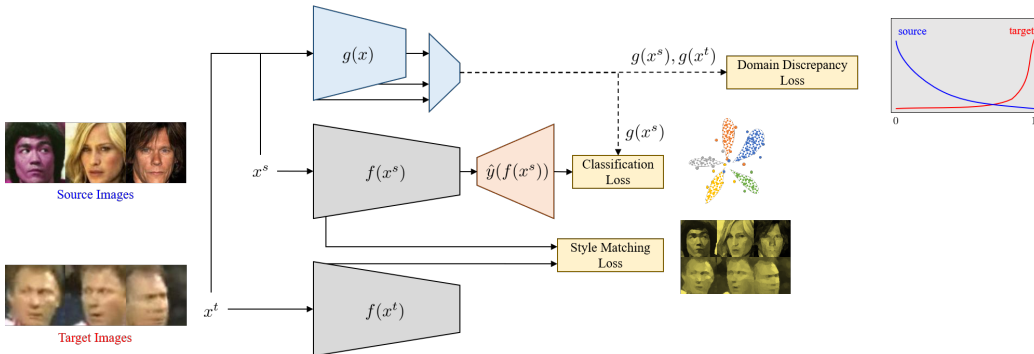
Figure 1: Style-based domain adaptation. The domain discriminator $g(x)$ is trained using domain discrepancy loss to score source images and up-weight samples with higher scores in classification loss. Style features are extracted from low-level feature maps. Style matching loss finds a common style space in which the style distributions of two domains are aligned.

domain, and n^t images in the target domain. The source and target images are x_i^s and x_j^t respectively. Each x_i^s has a label y_i^s which uses one-hot encoding. The target image labels are unknown, reflecting the need for domain adaptation. To simplify the notation, x, x^s, and x^t stand for an arbitrary image, a source image, and a target image respectively.

In general face recognition, the source and target domain are not shared classes, and the task is fine-grained categorization. In this case, short feature distances between two images do not imply that they are visually similar. We account for this by treating domain mismatch as style mismatch. We propose two approaches under different perspectives: perceptual scoring (PS) and style matching (SM). We outline the proposed approach in Fig. 1. For PS we draw from Zhang et al. [17] in the use of a domain discriminator, which judges the domain discrepancy of an image through a perceptual metric, to facilitate the learning of source images which are visually similar to the target images. In SM, given a baseline face recognition model $f(x)$, we extract style features from convolutional feature maps, and align the distributions of style features from the two domains. Thus the face recognition model generates convolutional features with homogeneous styles and focuses on learning target-like source images to improve testing performance.

The rest of this section is structured as follows. In the next subsection, we describe the primary classification loss with which we train the model by source images with the supervision of labels. In the second and third

subsections, we describe the PS and SM methods respectively, after which we summarize the two style-based domain adaptation methods.

3.1. Classification Loss

For visual recognition, the goal of an embedding function is to encode images to an embedding space in which similar images are close together and dissimilar images are far apart so that we can judge how similar two given images are, or which category an image belongs to. The easiest way to train an embedding function is to use an additional classifier. The embedding function is modeled by a convolutional neural network, $f(x)$, and the classifier is a single-layer perceptron (a matrix) followed by softmax, $\hat{y}(f(x))$. Since the output of the classifier is a probability distribution, we train the cascaded model, $\hat{y}(f(x))$, by minimizing cross entropy. The training loss is expressed as

$$\mathcal{L}_c = -y^s \log \hat{y}(f(x^s)) \tag{1}$$

which is termed classification loss. We use this to train a baseline model from scratch and preserve inter-class distances when adapting the model.

3.2. Perceptual Scoring

Assuming that domain information is shared between two domains, we draw from Chu et al. [18], Wu et al. [19], and Liu et al. [20] by mining informative images in the training dataset to mitigate domain shift.

3.2.1. Domain Discriminator

The architecture from Zhang et al. [17] is modified as the domain discriminator, as shown in Fig. 2. This discriminator approximates human-level judgments to calculate a score that represents how similar an image is to the target domain. For image x, a feature stack is extracted from L_g layers of a backbone network $\mathcal{F}(x)$ and unit-normalized in the channel dimension, denoted by $\mathcal{F}^l(x) \in \mathbb{R}^{H_l \times W_l \times C_l}$ for layer l. Each $\mathcal{F}^l(x)$ is scaled by vector $u^l \in \mathbb{R}^{C_l}$ and summed channel-wise. We average spatially to yield a scalar representation $r^l \in \mathbb{R}^1$ on each layer:

$$r^l = \frac{1}{H_l W_l} \sum_{h,w} u^l \otimes \mathcal{F}^l_{hw}(x) \tag{2}$$

where $\otimes$ is a convolution operator. We then concatenate the representations to produce a perceptual feature $r \in \mathbb{R}^{L_g}$, which we pass through a single-layer perceptron (vector v) followed by a sigmoid activation to judge the input image. The domain discriminator $g(x)$ is expressed as

$$g(x) = \frac{1}{1 + e^{-v^T r}}. \tag{3}$$

Note that since we use SqueezeNet [63] as the backbone network, in our case $L_g = 7$.
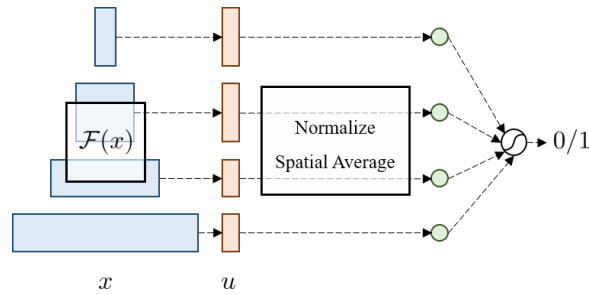

Figure 2: Domain discriminator $g(x)$, modified from Zhang et al. [17]. The backbone $\mathcal{F}(x)$ of $g(x)$ is SqueezeNet [63].

3.2.2. Training and Adaptation

We sample images from the source and target domains equally and use the following loss function (domain discrepancy loss) to train the domain discriminator:

$$\mathcal{L}_d = g^2(x^s) + (g(x^t) - 1)^2, \tag{4}$$

in which we expect the discriminator to produce a low score (tending to 0) for a source image but a high score (tending to 1) for a target image. This score is used in the classification loss in Equation 1 to up-weight the loss caused by target-like images. The classification loss is modified as

$$\mathcal{L}_c^* = g(x^s)\mathcal{L}_c, \tag{5}$$

where $\mathcal{L}_c^*$ is the loss for adapting the model based on PS.

3.3. Style Matching

Although PS indirectly reduces domain shift, its premise limits performance due to a lack of target-like images in the training dataset. To compensate for this weakness, with SM we seek a common space in which the style distributions of two domains are aligned.

9

3.3.1. Style Measures

According to studies on style transfer [21, 22, 23, 15], the stacks of mean and standard deviation on the feature maps describe the style of an image. For layer l in the face recognition model, the style representation is designated as $\{\mu(f^l(x)), \sigma(f^l(x))\}$. The measures of styles from the two domains are defined as

$$p_\mu^l \stackrel{def.}{=} \frac{1}{n^s} \sum_{i=1}^{n^s} \delta_{\mu(f^l(x_i^s))}, \ p_\sigma^l \stackrel{def.}{=} \frac{1}{n^s} \sum_{i=1}^{n^s} \delta_{\sigma(f^l(x_i^s))} \tag{6}$$

$$q_\mu^l \stackrel{def.}{=} \frac{1}{n^t} \sum_{j=1}^{n^t} \delta_{\mu(f^l(x_j^t))}, \ q_\sigma^l \stackrel{def.}{=} \frac{1}{n^t} \sum_{j=1}^{n^t} \delta_{\sigma(f^l(x_j^t))}, \tag{7}$$

where p_μ^l and p_σ^l are measures of $\{\mu(f^l(x^s)), \sigma(f^l(x^s))\}$, and q_μ^l and q_σ^l are measures of $\{\mu(f^l(x^t)), \sigma(f^l(x^t))\}$. We seek to minimize a certain distribution matching loss between $\{p_\mu^l, p_\sigma^l\}$, and $\{q_\mu^l, q_\sigma^l\}$.

3.3.2. Matching Distribution

In the literature on domain adaptation, MMD and adversarial learning are the main ways to match distributions. Although MMD is simple and necessitates no extra training parameters, it focuses on matching the region of high density [27], which may incur greater bias. Adversarial learning approaches, however, approximate relative entropy or the Wasserstein distance (optimal transport) by training the embedding function and the discriminator interactively. Although adversarial learning yields a better estimation of domain discrepancy, it requires extra parametric subnetworks, which complicates training. We strike a balance between the two methods by calculating the distribution matching loss using Sinkhorn divergence [24, 25, 26, 27, 28, 29, 30], which interpolates optimal transport and MMD, and has been successfully applied to generative models in Genevay et al. [64].

3.3.3. Sinkhorn Divergence

Similar to Genevay et al. [64], we align the style distributions of the source and target domains by minimizing

$$\mathcal{W}_\varepsilon(\mathcal{P}, \mathcal{Q}) = \min_{P \in \mathbb{R}_+^{n \times m}; \ P\mathbf{1}_m = \mathbf{1}_n; \ P^T \mathbf{1}_n = \mathbf{1}_m} \langle P, \hat{c} \rangle, \tag{8}$$

where $\hat{c} \stackrel{def.}{=} [c(z_i^\mathcal{P}, z_j^\mathcal{Q})]_{i,j} \in \mathbb{R}^{n \times m}$. Here, $z_i^\mathcal{P}$ and $z_j^\mathcal{Q}$ are samples from distributions $\mathcal{P}$ and $\mathcal{Q}$ respectively. Where $p > 0$ is some exponent, $c(z_i^\mathcal{P}, z_j^\mathcal{Q}) =$

$d(z_i^{\mathcal{P}}, z_j^{\mathcal{Q}})^p$ is a cost equipped with a distance function d. We define d as Euclidean distance, and set $p = 2$. The entropy-regularized optimal transport, that is, Wasserstein distance, is $\mathcal{W}_\varepsilon(\mathcal{P}, \mathcal{Q})$, in which factor ε regularizes entropy. Thus P can be treated as a mass-moving plan between $\mathcal{P}$ and $\mathcal{Q}$. As expressed in Cuturi [24], Cuturi and Doucet [25], and Genevay et al. [64], regularized optimal transport is equivalent to restricting the search space by using the scaling form of P:

$$P_{i,j} = a_i K_{i,j} b_j, \tag{9}$$

where $K_{i,j} \overset{def.}{=} e^{\frac{-\hat{c}_{i,j}}{\varepsilon}}$; the role of ε here mirrors that of bandwidth in MMD. The optimization problem of Equation 8 turns into finding a and b that meet certain requirements. Based on the Sinkhorn algorithm [24, 25], a and b can be found by

$$a_{l+1} \overset{def.}{=} \frac{\mathbf{1}_n}{K b_l} \quad \text{and} \quad b_{l+1} \overset{def.}{=} \frac{\mathbf{1}_m}{K^T a_{l+1}}, \tag{10}$$

where the fraction here is element-wise division. Starting with $b_0 = \mathbf{1}_m$, we obtain feasible a_L and b_L after L iterations. The budget L is set to 10 according to Genevay et al. [64]. Hence, Equation 8 can be modified as

$$\mathcal{W}_\varepsilon(\mathcal{P}, \mathcal{Q}) = \frac{1}{nm} a_L^T (K \odot \hat{c}) b_L, \tag{11}$$

where $\odot$ is an element-wise multiplication operator. Since $\hat{c}$ can be large, to prevent numerical explosions during training, we divide by nm to normalize the total cost. However, such a discrepancy approximation tends to overfit. To account for this, we add intra-measure Wasserstein distance to penalize the inter-measure Wasserstein distance:

$$\tilde{\mathcal{W}}_\varepsilon(\mathcal{P}, \mathcal{Q}) = 2\mathcal{W}_\varepsilon(\mathcal{P}, \mathcal{Q}) - \mathcal{W}_\varepsilon(\mathcal{P}, \mathcal{P}) - \mathcal{W}_\varepsilon(\mathcal{Q}, \mathcal{Q}), \tag{12}$$

where $\tilde{\mathcal{W}}_\varepsilon(\mathcal{P}, \mathcal{Q})$ is called Sinkhorn loss in Genevary et al. [64].

3.3.4. Style Matching Loss

We adopt Sinkhorn loss in Equation 12 to match the style distributions of the source and target domains, so the style matching loss can be expressed as

$$\mathcal{L}_s = \sum_{l=1}^{L_f} \tilde{\mathcal{W}}_\varepsilon(p_\mu^l, q_\mu^l) + \tilde{\mathcal{W}}_\varepsilon(p_\sigma^l, q_\sigma^l), \tag{13}$$

where L_f is the number of adaptation layers in $f(x)$.

3.4. Style-based Adaptation

Since style matching loss in Equation 13 requires the supervision of classification loss to learn categorization, adaptation loss with style matching is defined as

$$\mathcal{L} = \mathcal{L}_c + \lambda \mathcal{L}_s \tag{14}$$

where λ is a Lagrange multiplier. In the experiments, to prevent $\mathcal{L}_s$ from dominating the total loss, we set $\lambda = 0.01$ to make the product of $\lambda \mathcal{L}_s$ less than $\mathcal{L}_c$. The complete loss proposed in this paper consists of both PS and SM:

$$\mathcal{L}^* = \mathcal{L}_c^* + \lambda \mathcal{L}_s. \tag{15}$$

By minimizing $\mathcal{L}^*$, we adapt a model from the source domain to the target domain from a style perspective.

4. Evaluations

The two major applications of face recognition are face verification and identification, of which face identification further divides into closed-set and open-set identification. The performance of a model across different scenarios must be evaluated under different protocols.

4.1. Verification

The task of verification is to judge whether the given two facial images are the same identity. The two major evaluation protocols are described below.

4.1.1. K-fold Cross Validation

In this protocol, to avoid bias, the numbers of positive and negative pairs are usually the same, such as in the Labeled Faces in the Wild (LFW) [35, 65] and YouTube Faces (YTF) [66] datasets. The dataset is divided into K partitions. We evaluate the model on each partition by using the optimal threshold found by testing all the other partitions, and average the accuracies.

4.1.2. True Positive Rate under False Positive Rate

We determine the threshold for rejecting negative pairs that corresponds to the desired false positive rate (FPR) or false alarm rate (FAR), which yields a true positive rate (TPR) that represents the accuracy on positive pairs. In general, there are far more negative pairs than positive pairs to test the robustness of a model.

4.2. Closed-set Identification

Given a facial image, usually called the probe, the goal of face identification is to determine its identity by finding the most similar facial images in a gallery. In the case of closed-set identification, the identities of the probes must be a subset of the identities in the gallery. Therefore, rank-K (or top-K) accuracy is employed to evaluate the performance under this scenario. For each probe, we compute the similarities of all images in the gallery with respect to the probe, and sort these similarities from high to low. If the similarity between the probe and images of the same identity is ranked in the top-K, this identity is taken to be the correct prediction. After testing all the probes, rank-K accuracy is obtained as the ratio of correct predictions.

4.3. Open-set Identification

In open-set identification, the identities of probes may not be found in the gallery, in which case the task is not only to determine the identity of a given probe but also to report failure if the identity of the probe is not enrolled in the gallery. To evaluate the performance of open-set identification, we first set a threshold by which to reject probes with unknown identities under an acceptable FAR; in this case, this is the false positive identification rate (FPIR). Based on the set threshold, our metric is rank-1 accuracy, that is, the true positive identification rate (TPIR).

5. Experiments

5.1. Datasets

The datasets utilized here are listed in Table 1. Created for different purposes, they can be divided into three types:

5.1.1. Training

VGGFace2 [67] and CASIA-WebFace [68] are our training datasets; all facial images in both datasets were captured in the wild. Due to the large number of images for each identity in VGGFace2, it ensures better learning than CASIA-WebFace, even though it contains fewer identities. As in most of the relevant literature [6, 2, 3, 4], CASIA-WebFace is a primary source dataset in this paper. Following Wang et al. [3] and Arachchilage and Izquierdo [8], we initialize the backbone model on VGGFace2 after which we fine-tune the parameters on CASIA-WebFace.

5.1.2. Validation

We use LFW [35], CFP-FP [69], and AgeDB-30 [70] as the validation datasets; for each we use a 10-fold cross validation protocol. Their small size facilitates efficient model evaluations. When training a baseline model, we test it on these datasets after every epoch. After training, we pick the model whose average accuracy is the highest of all the generations as the baseline model.

5.1.3. Testing

IJB-A [31] is a joint face detection and recognition dataset that contains a mixture of still images and videos under challenging conditions, including blur as well as large pose and illumination variation. It provides 10-split evaluation protocols containing both verification and identification. We take the average of the 10-split evaluations as the final results. IJB-A was extended as IJB-B [32], which was further extended as IJB-C [33]. The evaluation methods in IJB-B and IJB-C are the same. In terms of verification, only one protocol is provided, but the positive-versus-negative pairs in IJB-B and IJB-C are about 10K/8M and 19.6K/15.6M respectively, which is more challenging than that of IJB-A (1.8K/10K), as listed in Table 2. For identification, both provide one probe set and two gallery sets for evaluation. We successively test each gallery set using the probe set and use their average as the final result. YTF [66] contains 3,425 videos from 1,595 identities, for a total of 621.2K frames. As with the validation datasets, its protocol follows 10-fold cross validation, in which each fold is composed of 250 positive and negative pairs. Furthermore, we cooperate with the library of National Chiao Tung University (NCTU) for surveillance application. A system was built to collect the data automatically. When a subject entered the library, the system recorded and labeled the video by the student or staff identity card. Due to personal information protection, the labels are anonymous. To eliminate the interference of head pose variation, we adopted the head pose estimation model in Hsu et al. [71] to filter out the frames with large head pose (pitch, roll, or yaw $> 15°$). This dataset is called NCTU-Lib, and its samples are shown in Fig. 3. The domain discrepancy between the training dataset and NCTU-Lib is large since almost all subjects in NCTU-Lib are Asian, which makes it more difficult to adapt the model.

Table 1: Training and testing datasets.Ver=verification, ID=identification.

Dataset	Protocol		Identities	Images	Images/identity
	Ver	ID			
VGGFace2 [67]			9,131	3.31M	362.6
CASIA-WebFace [68]			10,575	494.4K	46.8
LFW [35]	✓		5,749	13,233	2.3
CFP-FP [69]	✓		500	7,000	14
AgeDB-30 [70]	✓		568	16,488	29
IJB-A [31]	✓	✓	500	25.8K	51.6
IJB-B [32]	✓	✓	1,845	76.8K	41.6
IJB-C [33]	✓	✓	3,531	148.8K	42.1
YTF [66]	✓		1,595	621.2K	389.5
NCTU-Lib	✓	✓	6,187	105.1K	17.0

Table 2: Evaluation protocols on the testing datasets.

Dataset	Verification		Identification		
	Positive Pairs	Negative Pairs	Subjects (Gallery)	Samples/Subjects (Probe)	
				Known	Unknown
YTF [66]	250	250	-	-	
IJB-A [31]	1.8K	10K	112	1.2K/112	0.6K/55
IJB-B [32]	10K	8M	922	5.1K/922	5.1K/922
IJB-C [33]	19.6K	15.6M	1.77K	9.8K/1.77K	9.8K/1.8K
NCTU-Lib	4.4K	3.2M	3.16K	6.0K/3.16K	3.0K/3.0K

Figure 3: Samples in NCTU-Lib dataset. Due to personal information protection, their eyes are masked.

5.2. Implementation Details

Here, we describe the image preprocessing, feature processing, baseline model training, source and target dataset definitions, and training using the proposed domain adaptation methods.

5.2.1. Processing of Images and Features

If the multitask convolutional neural network (MTCNN) [72] detects a face in an image, we align the face to the fixed reference points using the eyes, mouth corners, and nose center. If it fails, we decide what to do based on the dataset. We ignore the training datasets and YTF since there is plenty of data for training and testing. For IJB-A/B/C, if three landmarks (eyes and nose center) are provided, we align these to the same reference points of the same landmarks, or we apply a square box whose side is half of the maximal side of the image to crop on the center. All processed images are resized to 128×128 and cropped to 112×112 for testing. When training, we augment the images by mirroring them with 50% probability, and resize them to 128×128 and randomly crop them to 112×112. In evaluations, we follow Whitelam et al. [32] when fusing the features. That is, in a template, the frames of each type of media (still images or video frames) are averaged before all medias are averaged.

5.2.2. Baseline Model and Source Dataset

We used MobileFaceNet [73] as our backbone model. Equation 1 is the primary classification loss in this paper. As mentioned above, the model was first trained on VGGFace2 dataset [67]. We used stochastic gradient descent (SGD) with momentum to train all models. The training epochs, batch size, learning rate, and momentum were set to 50, 128, 0.1, and 0.9 respectively, and the learning rate was divided by 10 every 12 epochs. After that, when transferring to CASIA-WebFace dataset [68], the learning rate was set to 0.01 to warm up the classifier $\hat{y}$ by one epoch before fine-tuning all parameters. We then set the learning rate to 0.0001 to fine-tune the parameters, and again divided by 10 every 12 epochs. The other settings remained unchanged. The backbone model fine-tuned on CASIA-WebFace was then used as the baseline model denoted by softmax.

5.2.3. Target Dataset

We assumed that the IJB-A/B/C datasets [31, 32, 33] are shared domain information. Only IJB-A was used as the target dataset when testing on

these datasets. We used all images and frames in IJB-A to adapt the model. Similarly, when testing on the YTF dataset [66], we used all the frames of each video in YTF. During adaptation, the learning rate was also set to 0.0001 to fine-tune the baseline model; other settings remained unchanged.

5.2.4. Regularizing Entropy for Style Matching

Since the role of ε is similar to bandwidth in MMD, we followed related studies [74, 2, 3] to set its value. Luo et al. [2] and Wang et al. [3] suggest setting the bandwidth to the median pairwise distance on source dataset. However, such an exhaustive search is not practical since training datasets are usually large. This can instead be estimated by a Monte Carlo method, but we propose a more efficient way to determine the value. Similar to the learning process in batch normalization, we estimated ε by the mean pairwise distance between source and target samples in a mini-batch, and updated it every iteration by

$$\varepsilon_{k+1} = \rho\varepsilon_k + (1 - \rho)\hat{\varepsilon}_k, \tag{16}$$

where $\hat{\varepsilon}_k$ is the current estimation. Momentum ρ was set to 0.9. In the following experiments, we compare the dynamic ε (the proposed method) and the fixed ε.

5.2.5. Definition of Adaptation Layers

MobileFaceNet [73] is described in Table 3. For the following experiments, we mainly used four adaptation layers in shallow networks for SM. From shallow to deep, the dimensions of the feature maps were $56^2 \times 64$ ($l = 1$), $28^2 \times 64$ ($l = 2$), $28^2 \times 64$ ($l = 3$), and $14^2 \times 128$ ($l = 4$) respectively.

5.3. Ablation Study

We analyzed our approaches using IJB-A as the target dataset, and evaluated the performance on IJB-A/B/C. The testing results are reported in Tables 4 and 5.

5.3.1. Effectiveness of Perceptual Scoring

The softmax PS method in Tables 4 and 5 is the proposed PS method described in Equation 5. Compared with the baseline, it yields improved performance. We also adopted pure SqueezeNet [63] as a discriminator, denoted as softmax FF PS, in which FF stands for feed-forward. There is no significant difference between the two methods, but results show that softmax PS is robust to false alarms, which implies that low-level features are important

Table 3: MobileFaceNet architecture [73] and proposed layer index definitions for adaptation

Operator	Input	Output	l
Convolution 3×3	$112^2 \times 3$	$56^2 \times 64$	-
Depth-wise convolution 3×3	$56^2 \times 64$	$56^2 \times 64$	1
Bottleneck $\times 1$	$56^2 \times 64$	$28^2 \times 64$	2
Bottleneck $\times 4$	$28^2 \times 64$	$28^2 \times 64$	3
Bottleneck $\times 1$	$28^2 \times 64$	$14^2 \times 128$	4
Bottleneck $\times 6$	$14^2 \times 128$	$14^2 \times 128$	5
Bottleneck $\times 1$	$14^2 \times 128$	$7^2 \times 128$	6
Bottleneck $\times 2$	$7^2 \times 128$	$7^2 \times 128$	7
Convolution 1×1	$7^2 \times 128$	$7^2 \times 512$	8
Linear depth-wise convolution 7×7	$7^2 \times 512$	$1^2 \times 512$	9
Linear convolution 1×1	$1^2 \times 512$	$1^2 \times 128$	10

Table 4: Verification performance on IJB-A/B/C [31, 32, 33] for ablation experiments. The values in boldface are the best in the row, and underlined values in boldface are the best in the column.

Method	IJB-A TPR (%)				IJB-B TPR (%)				IJB-C TPR (%)			
	FPR=0.0001	FPR=0.001	FPR=0.01	FPR=0.1	FPR=0.0001	FPR=0.001	FPR=0.01	FPR=0.1	FPR=0.0001	FPR=0.001	FPR=0.01	FPR=0.1
Baseline												
softmax	52.23	75.63	90.54	96.88	68.91	83.61	93.43	98.22	74.04	86.44	94.59	98.54
Perceptual scoring												
softmax FF PS	54.60	77.67	91.02	96.88	70.29	84.15	93.74	**98.32**	75.02	87.00	**94.92**	**98.61**
softmax PS	**55.00**	**78.43**	**91.17**	**96.92**	**71.16**	**84.58**	**93.75**	98.27	**75.82**	**87.21**	94.90	98.58
Style matching												
softmax SM ($L_f = 1$, fixed ε)	65.64	82.72	92.46	**96.96**	74.65	86.69	95.02	98.42	78.68	89.17	95.90	98.75
softmax SM ($L_f = 1$)	64.83	82.28	92.23	**96.96**	75.09	86.86	94.99	98.45	78.98	89.30	95.86	98.72
softmax SM ($L_f = 2$)	65.81	**83.67**	**92.48**	96.92	74.83	86.97	**95.08**	**98.49**	79.15	89.50	**95.94**	**98.76**
softmax SM ($L_f = 3$)	66.33	82.49	92.06	96.91	**75.58**	87.08	94.89	98.38	79.46	89.51	95.80	98.71
softmax SM ($L_f = 4$)	**67.64**	83.28	92.23	96.89	74.95	**87.22**	94.93	98.43	**79.81**	**89.58**	95.83	98.75
Combination												
softmax SM ($L_f = 1$) + PS	66.88	83.53	92.48	<u>**97.05**</u>	75.24	87.06	<u>**95.15**</u>	98.47	79.76	89.56	<u>**96.07**</u>	98.78
softmax SM ($L_f = 2$) + PS	67.78	<u>**84.31**</u>	<u>**92.65**</u>	97.03	<u>**75.96**</u>	<u>**87.55**</u>	95.08	<u>**98.50**</u>	<u>**80.19**</u>	<u>**89.85**</u>	95.99	<u>**98.79**</u>
softmax SM ($L_f = 3$) + PS	<u>**68.70**</u>	83.52	92.30	96.82	75.51	87.32	95.00	98.48	79.83	89.83	95.92	98.78
softmax SM ($L_f = 4$) + PS	68.58	83.76	92.31	96.77	75.50	87.20	94.93	98.48	79.93	89.61	95.81	98.71

for distinguishing identities at a finer granularity. To analyze the effect of PS, domain discriminator $g(x)$ is used to judge all images in both the source and target datasets. The distributions are shown in Fig. 4: the two domains are clearly separable, which is evidence of domain discrepancy. The purpose of PS is to mitigate such discrepancy by scoring samples in the source domain. With Equation 5, the distribution of the source dataset is flatter: note the reduced discrepancy for CASIA-WebFace (Weighted) in Fig. 4.

5.3.2. Effectiveness of Style Matching

Compared with PS, all SM approaches yield improvements in most metrics under different protocols. We find no differences among the metrics

Table 5: Identification performance on IJB-A/B/C [31, 32, 33] for ablation experiments. The values in boldface are the best in the row, and underlined values in boldface are the best in the column.

Method	IJB-A TPIR (%)				IJB-B TPIR (%)				IJB-C TPIR (%)			
	FPIR=0.01	FPIR=0.1	Rank-1	Rank-10	FPIR=0.01	FPIR=0.1	Rank-1	Rank-10	FPIR=0.01	FPIR=0.1	Rank-1	Rank-10
Baseline												
softmax	65.31	85.74	94.79	97.91	59.77	77.10	88.01	95.22	58.86	76.49	88.93	95.07
Perceptual scoring												
softmax FF PS	67.44	86.80	**95.28**	**98.02**	**61.79**	77.61	**89.54**	**95.29**	61.34	**77.94**	88.48	**95.32**
softmax PS	**68.78**	**86.95**	95.09	98.00	61.76	**77.98**	88.42	95.28	**62.18**	77.76	**89.35**	95.29
Style matching												
softmax SM ($L_f = 1$, fixed ε)	76.28	**89.35**	95.13	**98.11**	64.44	80.42	88.29	95.61	64.90	80.32	89.68	95.55
softmax SM ($L_f = 1$)	76.14	89.06	95.17	98.02	65.85	79.98	88.34	95.50	66.07	80.26	89.71	95.60
softmax SM ($L_f = 2$)	**76.59**	89.14	95.10	98.03	64.77	80.43	88.42	95.56	66.68	80.68	89.74	**95.61**
softmax SM ($L_f = 3$)	76.06	89.05	**95.20**	98.08	**66.25**	80.09	88.38	**95.66**	**67.55**	80.49	89.74	95.57
softmax SM ($L_f = 4$)	75.95	89.07	95.05	98.09	65.69	**80.63**	**88.77**	95.56	67.50	**80.73**	**89.75**	95.51
Combination												
softmax SM ($L_f = 1$) + PS	77.35	89.43	<u>**95.32**</u>	98.05	65.49	80.52	88.77	95.67	66.64	80.81	<u>**89.98**</u>	95.62
softmax SM ($L_f = 2$) + PS	<u>**77.62**</u>	<u>**89.65**</u>	95.15	<u>**98.16**</u>	65.85	<u>**80.87**</u>	<u>**88.85**</u>	95.73	68.05	<u>**81.20**</u>	<u>**89.98**</u>	<u>**95.74**</u>
softmax SM ($L_f = 3$) + PS	77.35	89.06	95.10	98.00	**65.94**	80.72	88.61	<u>**95.75**</u>	<u>**68.22**</u>	80.94	89.90	95.73
softmax SM ($L_f = 4$) + PS	76.83	89.02	95.16	98.02	65.30	80.50	88.80	95.66	68.07	80.98	89.89	95.65

Table 6: Statistics for embeddings in IJB-A [31]

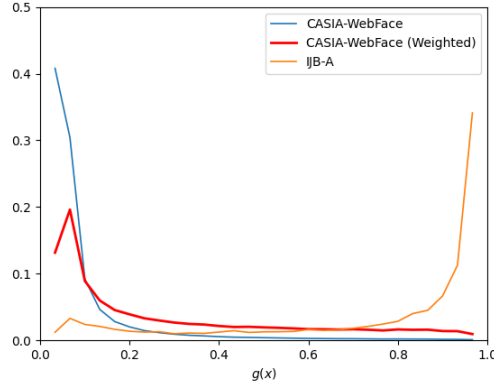| Method	Cosine similarity		Norm
	Intra-class	Inter-class	
softmax	0.7074 ± 0.1325	0.0728 ± 0.1161	113.89 ± 14.30
softmax PS	0.7071 ± 0.1330	0.0703 ± 0.1151	115.93 ± 13.76
softmax SM ($L_f = 2$)	0.6824 ± 0.1451	0.0191 ± 0.1103	118.21 ± 14.57
softmax SM ($L_f = 2$) + PS	0.6836 ± 0.1445	0.0188 ± 0.1101	119.09 ± 14.17

Figure 4: Distributions of $g(x^s)$ and $g(x^t)$ under CASIA-WebFace [68] and IJB-A [31], and the weighted distribution of CASIA-WebFace

when varying the adaptation layers L_f, but we do note a trend in which TPR or TPIR under lower FAR is better when more adaptation layers are

applied. However, there is no clear benefit to a fixed ε. It is slightly better for some metrics but worse on others. Conversely, using a dynamic ε is more convenient, and yields similar performance.

5.3.3. Combination of Perceptual Scoring and Style Matching

The performance of SM is further improved by PS. Improvements are more obvious on verification protocols. The improvements on identification protocols are slight but consistent. That is, most of the metrics show improvements. In particular, distinct improvements can be found in lower FAR (FPR and FPIR), which is an important concern in real-world scenarios. This implies that PS does help to generalize the learning of style matching on the target domain. Since most of the best metrics are achieved by $L_f = 2$, we adopt this as our default setting.

5.3.4. Embedding Analysis

To understand how the proposed methods affect the embedding space, we measure the embedding norm and inter-class and intra-class cosine similarities on the target datasets, as listed in Table 6. The norm measures the discriminative power of an embedding. PS slightly increases both the inter-class similarity and the embedding norm while preserving the intra-class similarity. SM separates embeddings from different classes by a large margin. Although intra-class similarity is decreased, the performance is also improved by larger inter-class similarity. In fact, the number of negative samples dominates in the testing protocols, which is a reasonable hypothesis in real-world applications; thus, slightly enlarging inter-class distances yields distinct improvements on accuracy. However, lower intra-class similarity saturates the performance at higher FAR, as shown in Tables 4 and 5. SM equipped with PS enjoys the benefits of both: not only is inter-class separation further enlarged, but intra-class similarity is also preserved slightly.

5.4. Benchmark Comparison

To adapt our baseline model to ensure a fair comparison, we implemented batch-instance normalization (BIN) [60] and multi-kernel MMD ($MMD_{m9,10}$) [2]. Subscripts 9 and 10 indicate that the multi-kernel MMD is applied to layers $l = 9$ and $l = 10$, as listed in Table 3. Evaluation on the YTF [66] dataset reveals that the proposed approach yields improvements over the baseline of more than 1%, which is the best of all methods under this benchmark. When BIN is applied on the baseline model, we find that it generalizes poorly.

20

Table 7: Benchmark comparison of verification performance on IJB-A/B/C [31, 32, 33]. The values in boldface are the best under the softmax baseline, and underlined values in boldface are the best in the column.

Method	IJB-A TPR (%)				IJB-B TPR (%)				IJB-C TPR (%)			
	FPR=0.0001	FPR=0.001	FPR=0.01	FPR=0.1	FPR=0.0001	FPR=0.001	FPR=0.01	FPR=0.1	FPR=0.0001	FPR=0.001	FPR=0.01	FPR=0.1
Sohn et al. [6]	-	58.40	82.80	96.20	-	-	-	-	-	-	-	-
IMAN-A [4]	-	84.49	91.88	97.05	-	-	-	-	-	-	-	-
CDA (vgg-soft) [3]	-	74.76	89.76	98.19	-	-	-	-	-	-	-	-
CDA (res-arc) [3]	-	82.45	91.11	96.96	-	87.35	94.55	98.08	-	88.06	94.85	98.33
softmax	52.23	75.63	90.54	96.88	68.91	83.61	93.43	98.22	74.04	86.44	94.59	98.54
softmax BIN [60]	59.17	76.17	89.48	96.22	68.48	82.29	92.62	98.16	73.00	85.04	94.02	98.52
softmax $MMD_{m9,10}$ [2]	65.64	83.50	92.35	97.02	75.00	86.83	94.88	98.54	79.18	89.29	95.86	98.84
softmax SM ($L_f=2$) + PS	67.78	84.31	92.65	97.03	75.96	87.55	95.08	98.50	80.19	89.85	95.99	98.79

Table 8: Benchmark comparison of identification performance on IJB-A/B/C [31, 32, 33]. The values in boldface are the best under the softmax baseline, and underlined values in boldface are the best in the column.

Method	IJB-A TPIR (%)				IJB-B TPIR (%)				IJB-C TPIR (%)			
	FPIR=0.01	FPIR=0.1	Rank-1	Rank-10	FPIR=0.01	FPIR=0.1	Rank-1	Rank-10	FPIR=0.01	FPIR=0.1	Rank-1	Rank-10
Sohn et al. [6]	-	-	87.90	97.00	-	-	-	-	-	-	-	-
IMAN-A [4]	-	-	94.05	98.04	-	-	-	-	-	-	-	-
CDA (vgg-soft) [3]	66.85	85.32	94.89	99.23	-	-	-	-	-	-	-	-
CDA (res-arc) [3]	75.49	87.76	93.61	97.62	-	-	86.22	93.33	-	-	88.19	93.70
softmax	65.31	85.74	94.79	97.91	59.77	77.10	88.01	95.22	58.86	76.49	88.93	95.07
softmax BIN [60]	67.91	84.17	94.33	97.92	61.29	75.10	86.33	94.63	61.43	75.13	87.51	94.68
softmax $MMD_{m9,10}$ [2]	76.40	89.21	95.21	98.07	64.23	80.07	88.35	95.40	65.80	80.44	89.73	95.54
softmax SM ($L_f=2$) + PS	77.62	89.65	95.15	98.16	65.85	80.87	88.85	95.73	68.05	81.20	89.98	95.74

Comprehensive testing results on IJB-A/B/C [31, 32, 33] are listed in Tables 7 and 8. We note that despite the weak capacity of our backbone model [73] (Wang et al. [3, 4] employ ResNet34 [75] as their primary backbone), our approach outperforms prior work, even that of Wang et al. [3], who guide ResNet using ArcFace [46]. Since performance at higher FAR is nearly all saturated, metrics at lower FAR become critical to judge the model's performance. These results show that the proposed approach outperforms most prior work.

Table 9: Benchmark comparison on YTF [66]. The value in boldface is the best in the column.

Method	Accuracy
Sohn et al. [6]	95.38
softmax	94.46
softmax BIN [60]	93.62
softmax $MMD_{m9,10}$ [2]	95.28
softmax SM ($L_f=2$) + PS	**95.52**

Table 10: Verification and identification performance on NCTU-Lib.
The values in boldface are the best in the row, and underlined values in boldface are the best in the column.

Method	# Subjects	Verification TPR (%)				Identification TPIR (%)			
		FPR=0.0001	FPR=0.001	FPR=0.01	FPR=0.1	FPIR=0.01	FPIR=0.1	Rank-1	Rank-10
softmax	-	76.00	87.20	94.73	99.13	45.60	68.49	84.97	94.40
softmax SM ($L_f = 2$)	1,000	80.74	**90.39**	96.64	**99.53**	49.92	**74.27**	**86.52**	95.36
	3,000	80.68	**90.39**	96.66	**99.53**	50.77	73.64	86.12	95.36
	5,000	**80.93**	90.29	96.53	99.52	51.48	73.64	86.40	**95.44**
softmax SM ($L_f = 2$) + PS	1,000	80.67	**90.50**	**96.84**	99.49	**51.74**	**74.62**	**86.59**	**95.49**
	3,000	80.44	90.04	96.65	99.43	50.45	73.79	85.95	95.22
	5,000	80.34	90.41	96.83	99.47	49.44	74.05	85.94	95.27

5.5. Application

We apply our approaches to NCTU-Lib dataset here. To simulate the real situation, we sampled 1,000, 3,000, and 5,000 subjects to be target datasets. As we can see in Table 10, no matter how many subjects are trained, the proposed approaches can improve the baseline model significantly, especially in lower FAR. The major differences can be observed easily in the results of open-set identification under FPIR=0.01. For softmax SM ($L_f = 2$), it is obvious that the improvements can be better with more subjects. After applying PS, however, the performance decays with the growing of subjects. We speculate the reason is a lack of target domain information in the training dataset. As shown in Fig. 5, with more subjects, it is easier for a discriminator $g(x)$ to distinguish two domains. The scores of most source images are then close to 0, which results in down-weighting the classification loss. Despite the drawback of PS, in Table 10, softmax SM ($L_f = 2$) + PS with 1,000 subjects, since the weak discriminator can not only up-weight the target-like images but also preserve the weights of others, it does help SM to train a better model with fewer subjects. Therefore, if the domain discrepancy is large, the discriminator cannot be too strong, or it may limit the performance.

6. Conclusion

In face recognition applications, classes do not overlap across domains; face recognition also involves fine-grained classification, and as such does not strictly follow the low-density separation principle. Together, these traits complicate the design of algorithms to reduce the domain gap. We treat domain mismatch as a style mismatch problem, and leverage texture-level features as the key to properly adapting a face recognition model to target domains. We propose perceptual scoring and style matching. The former

(a) # Subjects = 1000   (b) # Subjects = 3000   (c) # Subjects = 5000
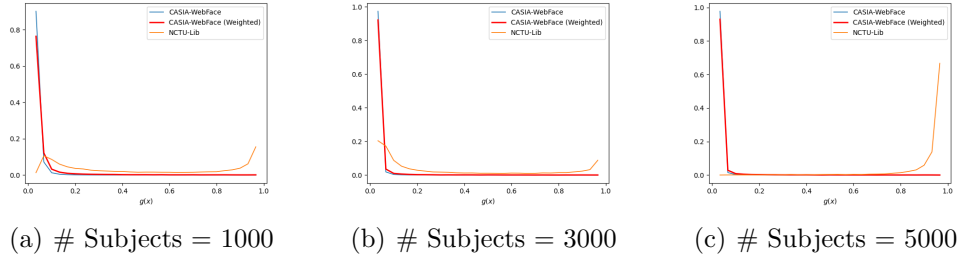
Figure 5: Distributions of $g(x^s)$ and $g(x^t)$ under CASIA-WebFace [68] and NCTU-Lib, and the weighted distribution of CASIA-WebFace.

mines visually target-like images in the training data to promote their learning, and the latter forces the learning of a common style space in which the style distributions of the two domains are confused, effectively normalizing the style of feature maps. We conduct evaluations using the protocols of face verification and closed-set and open-set identification, demonstrating that our approach has good domain transfer ability and even outperforms most prior work. This progress is due to larger inter-class variation. The intra-class similarity, however, is reduced, which could explain the performance saturation at higher false alarm rates. Thus future work will involve reducing inter-class similarity and increasing intra-class similarity simultaneously to achieve comprehensive improvements on the target domain.

Declaration of Competing Interest

The authors declare that they have no known competing financial interests or personal relationships that could have appeared to influence the work reported in this paper.

CRediT authorship contribution statement

Chun-Hsien Lin: Conceptuealization, Methodology, Software, Writing - Original Draft, Writing - Review & Editing, Data Curation, Formal analysis, Investigation.
Bing-Fei Wu: Supervision, Funding acquisition.

References

[1] P. J. Phillips, A cross benchmark assessment of a deep convolutional neural network for face recognition, in: 12th IEEE International Conference on Automatic Face & Gesture Recognition (FG 2017), IEEE, 2017, pp. 705–710.

[2] Z. Luo, J. Hu, W. Deng, H. Shen, Deep unsupervised domain adaptation for face recognition, in: 13th IEEE International Conference on Automatic Face & Gesture Recognition (FG 2018), IEEE, 2018, pp. 453–457.

[3] M. Wang, W. Deng, Deep face recognition with clustering based domain adaptation, Neurocomputing 393 (2020) 1–14.

[4] M. Wang, W. Deng, J. Hu, X. Tao, Y. Huang, Racial faces in the wild: Reducing racial bias by information maximization adaptation network, in: Proceedings of the IEEE/CVF International Conference on Computer Vision, 2019, pp. 692–702.

[5] S. W. Arachchilage, E. Izquierdo, SSDL: Self-supervised domain learning for improved face recognition, arXiv preprint arXiv:2011.13361 (2020).

[6] K. Sohn, S. Liu, G. Zhong, X. Yu, M.-H. Yang, M. Chandraker, Unsupervised domain adaptation for face recognition in unlabeled videos, in: Proceedings of the IEEE International Conference on Computer Vision, 2017, pp. 3210–3218.

[7] S. Hong, W. Im, J. Ryu, H. S. Yang, SSPP-DAN: Deep domain adaptation network for face recognition with single sample per person, in: 2017 IEEE International Conference on Image Processing (ICIP), IEEE, 2017, pp. 825–829.

[8] S. W. Arachchilage, E. Izquierdo, ClusterFace: Joint clustering and classification for set-based face recognition, arXiv preprint arXiv:2011.13360 (2020).

[9] J. Yosinski, J. Clune, Y. Bengio, H. Lipson, How transferable are features in deep neural networks?, arXiv preprint arXiv:1411.1792 (2014).

[10] K. Bousmalis, N. Silberman, D. Dohan, D. Erhan, D. Krishnan, Unsupervised pixel-level domain adaptation with generative adversarial networks, in: CVPR, 2017.

[11] L. Tran, K. Sohn, X. Yu, X. Liu, M. Chandraker, Gotta Adapt 'Em All: Joint pixel and feature-level domain adaptation for recognition in the wild, in: Proceedings of the IEEE/CVF Conference on Computer Vision and Pattern Recognition, 2019, pp. 2672–2681.

[12] R. Li, Q. Jiao, W. Cao, H.-S. Wong, S. Wu, Model adaptation: Unsupervised domain adaptation without source data, in: Proceedings of the IEEE/CVF Conference on Computer Vision and Pattern Recognition, 2020, pp. 9641–9650.

[13] I. J. Goodfellow, J. Pouget-Abadie, M. Mirza, B. Xu, D. Warde-Farley, S. Ozair, A. Courville, Y. Bengio, Generative adversarial networks, arXiv preprint arXiv:1406.2661 (2014).

[14] T. Karras, T. Aila, S. Laine, J. Lehtinen, Progressive growing of GANs for improved quality, stability, and variation, arXiv preprint arXiv:1710.10196 (2017).

[15] T. Karras, S. Laine, T. Aila, A style-based generator architecture for generative adversarial networks, in: Proceedings of the IEEE/CVF Conference on Computer Vision and Pattern Recognition, 2019, pp. 4401–4410.

[16] A. Tewari, M. Elgharib, G. Bharaj, F. Bernard, H.-P. Seidel, P. Pérez, M. Zollhofer, C. Theobalt, StyleRig: Rigging StyleGAN for 3D control over portrait images, in: Proceedings of the IEEE/CVF Conference on Computer Vision and Pattern Recognition, 2020, pp. 6142–6151.

[17] R. Zhang, P. Isola, A. A. Efros, E. Shechtman, O. Wang, The unreasonable effectiveness of deep features as a perceptual metric, in: Proceedings of the IEEE Conference on Computer Vision and Pattern Recognition, 2018, pp. 586–595.

[18] W.-S. Chu, F. De la Torre, J. F. Cohn, Selective transfer machine for personalized facial expression analysis, IEEE Transactions on Pattern Analysis and Machine Intelligence 39 (2016) 529–545.

[19] B.-F. Wu, C.-H. Lin, Adaptive feature mapping for customizing deep learning based facial expression recognition model, IEEE Access 6 (2018) 12451–12461.

[20] M. Liu, Y. Song, H. Zou, T. Zhang, Reinforced training data selection for domain adaptation, in: Proceedings of the 57th Annual Meeting of the Association for Computational Linguistics, 2019, pp. 1957–1968.

[21] D. Ulyanov, A. Vedaldi, V. Lempitsky, Improved texture networks: Maximizing quality and diversity in feed-forward stylization and texture synthesis, in: Proceedings of the IEEE Conference on Computer Vision and Pattern Recognition, 2017, pp. 6924–6932.

[22] V. Dumoulin, J. Shlens, M. Kudlur, A learned representation for artistic style, arXiv preprint arXiv:1610.07629 (2016).

[23] X. Huang, S. Belongie, Arbitrary style transfer in real-time with adaptive instance normalization, in: Proceedings of the IEEE International Conference on Computer Vision, 2017, pp. 1501–1510.

[24] M. Cuturi, Sinkhorn distances: lightspeed computation of optimal transport, in: NIPS, volume 2, 2013, p. 4.

[25] M. Cuturi, A. Doucet, Fast computation of Wasserstein barycenters, in: International Conference on Machine Learning, PMLR, 2014, pp. 685–693.

[26] G. Aude, M. Cuturi, G. Peyré, F. Bach, Stochastic optimization for large-scale optimal transport, arXiv preprint arXiv:1605.08527 (2016).

[27] J. Feydy, T. Séjourné, F.-X. Vialard, S.-i. Amari, A. Trouvé, G. Peyré, Interpolating between optimal transport and MMD using Sinkhorn divergences, in: 22nd International Conference on Artificial Intelligence and Statistics, PMLR, 2019, pp. 2681–2690.

[28] A. Genevay, L. Chizat, F. Bach, M. Cuturi, G. Peyré, Sample complexity of Sinkhorn divergences, in: 22nd International Conference on Artificial Intelligence and Statistics, PMLR, 2019, pp. 1574–1583.

[29] A. Genevay, Entropy-regularized optimal transport for machine learning, Ph.D. thesis, Paris Sciences et Lettres, 2019.

[30] L. Chizat, P. Roussillon, F. Léger, F.-X. Vialard, G. Peyré, Faster Wasserstein distance estimation with the Sinkhorn divergence, arXiv preprint arXiv:2006.08172 (2020).

[31] B. F. Klare, B. Klein, E. Taborsky, A. Blanton, J. Cheney, K. Allen, P. Grother, A. Mah, A. K. Jain, Pushing the frontiers of unconstrained face detection and recognition: IARPA Janus Benchmark A, in: Proceedings of the IEEE Conference on Computer Vision and Pattern Recognition, 2015, pp. 1931–1939.

[32] C. Whitelam, E. Taborsky, A. Blanton, B. Maze, J. Adams, T. Miller, N. Kalka, A. K. Jain, J. A. Duncan, K. Allen, et al., IARPA Janus Benchmark-B face dataset, in: Proceedings of the IEEE Conference on Computer Vision and Pattern Recognition Workshops, 2017, pp. 90–98.

[33] B. Maze, J. Adams, J. A. Duncan, N. Kalka, T. Miller, C. Otto, A. K. Jain, W. T. Niggel, J. Anderson, J. Cheney, et al., IARPA Janus Benchmark-C: Face dataset and protocol, in: International Conference on Biometrics (ICB), IEEE, 2018, pp. 158–165.

[34] Y. Taigman, M. Yang, M. Ranzato, L. Wolf, DeepFace: Closing the gap to human-level performance in face verification, in: Proceedings of the IEEE Conference on Computer Vision and Pattern Recognition, 2014, pp. 1701–1708.

[35] G. B. Huang, M. Ramesh, T. Berg, E. Learned-Miller, Labeled Faces in the Wild: A Database for Studying Face Recognition in Unconstrained Environments, Technical Report 07-49, University of Massachusetts, Amherst, 2007.

[36] I. Masi, Y. Wu, T. Hassner, P. Natarajan, Deep face recognition: A survey, in: 31st Conference on Graphics, Patterns and Images (SIBGRAPI), IEEE, 2018, pp. 471–478.

[37] W. Ouyang, P. Luo, X. Zeng, S. Qiu, Y. Tian, H. Li, S. Yang, Z. Wang, Y. Xiong, C. Qian, et al., DeepID-Net: Multi-stage and deformable deep convolutional neural networks for object detection, arXiv preprint arXiv:1409.3505 (2014).

[38] W. Ouyang, X. Wang, X. Zeng, S. Qiu, P. Luo, Y. Tian, H. Li, S. Yang, Z. Wang, C.-C. Loy, et al., DeepID-Net: Deformable deep convolutional neural networks for object detection, in: Proceedings of the IEEE Conference on Computer Vision and Pattern Recognition, 2015, pp. 2403–2412.

[39] W. Ouyang, X. Zeng, X. Wang, S. Qiu, P. Luo, Y. Tian, H. Li, S. Yang, Z. Wang, H. Li, et al., DeepID-Net: Object detection with deformable part based convolutional neural networks, IEEE Transactions on Pattern Analysis and Machine Intelligence 39 (2016) 1320–1334.

[40] R. Hadsell, S. Chopra, Y. LeCun, Dimensionality reduction by learning an invariant mapping, in: IEEE Computer Society Conference on Computer Vision and Pattern Recognition (CVPR'06), volume 2, IEEE, 2006, pp. 1735–1742.

[41] F. Schroff, D. Kalenichenko, J. Philbin, FaceNet: A unified embedding for face recognition and clustering, in: Proceedings of the IEEE Conference on Computer Vision and Pattern Recognition, 2015, pp. 815–823.

[42] M. Kaya, H. Ş. Bilge, Deep metric learning: A survey, Symmetry 11 (2019) 1066.

[43] Y. Wen, K. Zhang, Z. Li, Y. Qiao, A discriminative feature learning approach for deep face recognition, in: European Conference on Computer Vision, Springer, 2016, pp. 499–515.

[44] W. Liu, Y. Wen, Z. Yu, M. Li, B. Raj, L. Song, SphereFace: Deep hypersphere embedding for face recognition, in: Proceedings of the IEEE Conference on Computer Vision and Pattern Recognition, 2017, pp. 212–220.

[45] H. Wang, Y. Wang, Z. Zhou, X. Ji, D. Gong, J. Zhou, Z. Li, W. Liu, CosFace: Large margin cosine loss for deep face recognition, in: Proceedings of the IEEE Conference on Computer Vision and Pattern Recognition, 2018, pp. 5265–5274.

[46] J. Deng, J. Guo, N. Xue, S. Zafeiriou, ArcFace: Additive angular margin loss for deep face recognition, in: Proceedings of the IEEE/CVF Conference on Computer Vision and Pattern Recognition, 2019, pp. 4690–4699.

[47] H. Liu, X. Zhu, Z. Lei, S. Z. Li, AdaptiveFace: Adaptive margin and sampling for face recognition, in: Proceedings of the IEEE/CVF Conference on Computer Vision and Pattern Recognition, 2019, pp. 11947–11956.

[48] B. Liu, W. Deng, Y. Zhong, M. Wang, J. Hu, X. Tao, Y. Huang, Fair loss: Margin-aware reinforcement learning for deep face recognition, in: Proceedings of the IEEE/CVF International Conference on Computer Vision, 2019, pp. 10052–10061.

[49] Y. Huang, Y. Wang, Y. Tai, X. Liu, P. Shen, S. Li, J. Li, F. Huang, CurricularFace: Adaptive curriculum learning loss for deep face recognition, in: Proceedings of the IEEE/CVF Conference on Computer Vision and Pattern Recognition, 2020, pp. 5901–5910.

[50] M. Wang, W. Deng, Deep visual domain adaptation: A survey, Neurocomputing 312 (2018) 135–153.

[51] M. Long, Y. Cao, J. Wang, M. I. Jordan, Learning transferable features with deep adaptation networks, in: International Conference on Machine Learning, PMLR, 2015, pp. 97–105.

[52] B. Sun, K. Saenko, Deep CORAL: Correlation alignment for deep domain adaptation, in: European Conference on Computer Vision, Springer, 2016, pp. 443–450.

[53] M. Long, Y. Cao, Z. Cao, J. Wang, M. I. Jordan, Transferable representation learning with deep adaptation networks, IEEE Transactions on Pattern Analysis and Machine Intelligence 41 (2018) 3071–3085.

[54] Y. Ganin, V. Lempitsky, Unsupervised domain adaptation by backpropagation, in: International Conference on Machine Learning, PMLR, 2015, pp. 1180–1189.

[55] E. Tzeng, J. Hoffman, K. Saenko, T. Darrell, Adversarial discriminative domain adaptation, in: Proceedings of the IEEE Conference on Computer Vision and Pattern Recognition, 2017, pp. 7167–7176.

[56] X. Ma, T. Zhang, C. Xu, Deep multi-modality adversarial networks for unsupervised domain adaptation, IEEE Transactions on Multimedia 21 (2019) 2419–2431.

[57] H. Yan, Z. Li, Q. Wang, P. Li, Y. Xu, W. Zuo, Weighted and class-specific maximum mean discrepancy for unsupervised domain adaptation, IEEE Transactions on Multimedia 22 (2019) 2420–2433.

[58] Y. Li, N. Wang, J. Shi, J. Liu, X. Hou, Revisiting batch normalization for practical domain adaptation, arXiv preprint arXiv:1603.04779 (2016).

[59] Y. Qing, Y. Zhao, Y. Shi, D. Chen, Y. Lin, Y. Peng, Improve cross-domain face recognition with IBN-block, in: IEEE International Conference on Big Data (BIG DATA), IEEE, 2018, pp. 4613–4618.

[60] H. Nam, H.-E. Kim, Batch-instance normalization for adaptively style-invariant neural networks, arXiv preprint arXiv:1805.07925 (2018).

[61] C. Qian, Y. Jin, Y. Li, C. Lang, S. Feng, T. Wang, Deep domain adaptation for Asian face recognition via Ada-IBN, in: IEEE International Conference on Multimedia & Expo Workshops (ICMEW), IEEE, 2019, pp. 525–530.

[62] X. Jin, C. Lan, W. Zeng, Z. Chen, Style normalization and restitution for domain generalization and adaptation, arXiv preprint arXiv:2101.00588 (2021).

[63] F. N. Iandola, S. Han, M. W. Moskewicz, K. Ashraf, W. J. Dally, K. Keutzer, SqueezeNet: AlexNet-level accuracy with 50x fewer parameters and <0.5MB model size, arXiv preprint arXiv:1602.07360 (2016).

[64] A. Genevay, G. Peyré, M. Cuturi, Learning generative models with Sinkhorn divergences, in: International Conference on Artificial Intelligence and Statistics, PMLR, 2018, pp. 1608–1617.

[65] G. B. H. E. Learned-Miller, Labeled Faces in the Wild: Updates and New Reporting Procedures, Technical Report UM-CS-2014-003, University of Massachusetts, Amherst, 2014.

[66] L. Wolf, T. Hassner, I. Maoz, Face recognition in unconstrained videos with matched background similarity, in: CVPR 2011, IEEE, 2011, pp. 529–534.

[67] Q. Cao, L. Shen, W. Xie, O. M. Parkhi, A. Zisserman, VGGFace2: A dataset for recognising faces across pose and age, in: 13th IEEE international conference on automatic face & gesture recognition (FG 2018), IEEE, 2018, pp. 67–74.

[68] D. Yi, Z. Lei, S. Liao, S. Z. Li, Learning face representation from scratch, arXiv preprint arXiv:1411.7923 (2014).

[69] S. Sengupta, J.-C. Chen, C. Castillo, V. M. Patel, R. Chellappa, D. W. Jacobs, Frontal to profile face verification in the wild, in: 2016 IEEE Winter Conference on Applications of Computer Vision (WACV), IEEE, 2016, pp. 1–9.

[70] S. Moschoglou, A. Papaioannou, C. Sagonas, J. Deng, I. Kotsia, S. Zafeiriou, AgeDB: the first manually collected, in-the-wild age database, in: Proceedings of the IEEE Conference on Computer Vision and Pattern Recognition Workshops, 2017, pp. 51–59.

[71] H.-W. Hsu, T.-Y. Wu, S. Wan, W. H. Wong, C.-Y. Lee, Quatnet: Quaternion-based head pose estimation with multiregression loss, IEEE Transactions on Multimedia 21 (2018) 1035–1046.

[72] K. Zhang, Z. Zhang, Z. Li, Y. Qiao, Joint face detection and alignment using multitask cascaded convolutional networks, IEEE Signal Processing Letters 23 (2016) 1499–1503.

[73] S. Chen, Y. Liu, X. Gao, Z. Han, MobileFaceNets: Efficient CNNs for accurate real-time face verification on mobile devices, in: Chinese Conference on Biometric Recognition, Springer, 2018, pp. 428–438.

[74] A. Gretton, D. Sejdinovic, H. Strathmann, S. Balakrishnan, M. Pontil, K. Fukumizu, B. K. Sriperumbudur, Optimal kernel choice for large-scale two-sample tests, in: Advances in neural information processing systems, Citeseer, 2012, pp. 1205–1213.

[75] K. He, X. Zhang, S. Ren, J. Sun, Deep residual learning for image recognition, in: Proceedings of the IEEE Conference on Computer Vision and Pattern Recognition, 2016, pp. 770–778.